RESEARCH PAPER

Guoqing Hu · Yali Gao · Philip M. Sherman
Dongqing Li

A microfluidic chip for heterogeneous immunoassay using electrokinetical control

Abstract This article presents the development of a novel, automated, electrokinetically controlled heterogeneous immunoassay on a poly(dimethylsiloxane) (PDMS) microfluidic chip. A numerical method has been developed to simulate the electrokinetically driven, time-dependent delivery processes of reagents and washing solutions within the complex microchannel network. Based on the parameters determined from the numerical simulations, fully automated on-chip experiments to detect *Helicobacter pylori* were accomplished by sequentially changing the applied electric fields. Shortened assay time and much less reagent consumptions are achieved by using this microchannel chip while the detection limit is comparable to the conventional assay. There is a good agreement between the experimental result and numerical prediction, demonstrating the effectiveness of using CFD to assist the experimental studies of microfluidic immunoassay.

Keywords Microfluidics · Lab-on-a-chip · Heterogeneous immunoassay · Numerical simulation · *H. pylori* · Electroosmosis

1 Introduction

Immunoassays form the backbone for tests used in the study of infectious diseases and clinical endocrinology. They have been widely applied to a range of biological fields, e.g. viruses, bacteria, fungi since their first intro-

G. Hu · Y. Gao · D. Li (✉)
Department of Mechanical and Industrial Engineering,
University of Toronto, 5 King's College Road,
Toronto, ON, M5S 3G8, Canada
E-mail: dli@mie.utoronto.ca

P. M. Sherman
Departments of Paediatrics and Laboratory
Medicine & Pathobiology, University of Toronto,
Toronto, ON, Canada

duction in 1970s by Yalow and Berson (1959) for insulin and by Ekins (1960) for thyroxine. Immunoassay provides highly sensitive and precise methods for the detection of biological agents, with the added advantage that it can handle large numbers of samples that need to be analyzed. However, a conventional immunoassay test needs at least several hours to complete because it is a multistage, labor-intensive process (Sia and Whitesides 2003). Automation of immunoassay test generally requires a complex and cumbersome robotic technique for fluid handling, which is not only very expensive but also prevents immunoassay from being a tool for point of care testing (Dodge et al. 2001).

Miniaturization of laboratory processes is attractive since it allows for improved reaction kinetics, minimal reagent consumption, less waste production, automation and parallel processing (Knight Honey 2002). The microfluidic techniques developed during the last decade provide a very promising way to miniaturize immunoassays (Chiem and Harrison 1998; Dodge et al. 2001; Wang et al. 2001; Linder et al. 2002; Lin et al. 2004; Lai et al. 2004). One of the critical elements for microfluidic systems is the reagent transport. Electroosmosis and hydraulic pressure are two most commonly used fluid driving modes. Chiem and Harrison (1998) developed a homogeneous immunoassay for serum theophylline by using on-chip electrophoretic separation. Wang et al. (2001) demonstrated a microfluidic device for conducting electrochemical enzyme homogeneous immunoassays to detect the IgG model analyte. Dodge et al. (2001) designed a microfluidic platform for heterogeneous immunoassay in which the reagents are manually filled into reservoirs in each step and delivered using electrokinetic pumping. Linder et al. (2002) also used electrokinetically driven flow to conduct a competitive immunoassay for human IgG on a biopassivated cross microchannel. Lin et al. (2004) designed a new enzyme-linked immunosorbent assay (ELISA) strategy based on poly(dimethylsiloxane) (PDMS) microchannels for the detection of *Helicobacter pylori* infection. In their experiments, the delivery of reagent solutions through

the PDMS microchannels is accomplished by using pressure-driven flow. Lai et al. (2004) fabricated a microfluidic ELISA on a compact disk in which the delivery of reagent solutions are controlled by centrifugal and capillary forces.

Very large hydrodynamic pressure may be required to generate liquid flow in microfluidic devices, because the hydraulic resistance is reversely proportional to the fourth power of transverse channel dimension (Kovacs 2001). Therefore, this may become impractical. Alternatively, electrokinetic body forces can be utilized to drive liquid flow in microchannels, which is known as electroosmotic pumping (Harrison et al. 1993; Arulanandam and Li 2000). Because the channel wall in contact with an aqueous solution has electrostatic charge, these charges will attract the counterions in the liquid to form an electric double layer (EDL). When an external electrical field is applied along the channel length direction, the electrical field force drives the net charge in the EDL to move, resulting in a bulk liquid flow called electroosmotic flow. Electroosmotic pumping is suitable for transporting liquid in microchannels in a lab-chip device since this method does not involve moving parts, and does not produce pulsating flows. Furthermore, electroosmotic pumping generates a plug-like velocity profile, which is favorable for sample delivery, and the average velocity is independent of the microchannel size. Therefore, we choose the electroosmotic pumping for the delivery of the reagents and other solutions in the microfluidic immunoassay chip.

Analogous to the conventional indirect ELISA (Crowther 2001), present heterogeneous immunoassay analysis includes following multiple steps: (1) immobilizing (coating) the antigens onto microchannel walls; (2) loading the primary antibody solution and incubating; (3) washing away the unbound (free) primary antibody; (4) loading the secondary antibody and incubating; (5) washing away the unbound secondary antibody; and (6) detecting the signal from reaction. Step (1) is done prior to the immunoassay chip operation. The washing steps (3) and (5) are required to prevent non-specific protein interactions. The detection step (6) is conducted under microscope after the reaction. It should be noted that in the above-mentioned heterogeneous immunoassays (Dodge et al. 2000; Linder et al. 2002), although the sample delivery was realized by electroosmotic pumping, manual operations such as filling different reagents to different reservoirs were still required between analysis steps. In the present study, we have realized steps (2) to (5) by an automated electrokinetic means in a multi-microchannel network. To control such sequential loading and displacing processes for different reagent solutions, the duration of each operation, the applied electrical potentials needed for a specified solution, and the dimensions and electrokinetic properties of the microchannels must be known. This requires fundamental studies of these on-chip microfluidic processes. To our knowledge, no theoretical or numerical study on the entire operation of a multi-microchannel immunoassay chip has been reported so far.

Computational fluid dynamics (CFD) is a powerful tool to build virtual prototypes and simulate the performance of the proposed designs in many engineering fields. It allows experimentalists to reduce the number of experiments significantly using the information provided by computational simulations. There are many recently published papers on microfluidic problems using CFD (Ermakov et al. 1998; Stewart et al. 2001; Erickson and Li 2003). Due to the complexity of the microfluidic processes in the multi-microchannel immunoassay chip, it is difficult to find the optimal design and controlling parameters for the chip operations merely by experiments. Therefore it is necessary to apply the CFD method to design and analyze the entire on-chip microfluidic processes and thus realize precise control of the immunoassay.

In the present paper, we develop a two-dimensional numerical model, based on unstructured finite element methodology, for the electrokinetically driven flows and mass transport processes in a complex microchannel network. The sequential microfluidic operation steps and the sample transportation in an immunoassay analysis cycle are studied numerically. We also discuss the effect of the induced pressure-driven flow. Finally, we fabricate an integrated PDMS microfluidic immunoassay chip according to the results of our numerical simulation studies. We conduct immunoassay experiments to detect *H. pylori* antigen and obtain a comparable limit of detection to the corresponding conventional ELISA (Lin et al. 2004). The immunoassay operations are performed by switching the applied electric potential at prescribed time steps and therefore full automation of the microfluidic immunoassay is achieved.

2 Physical model and numerical method

We consider here the steady electroosmotic flow (EOF) and the transient sample transportation within a microchannel network. Generally, the steady state EOF will be established instantaneously (approximately several milliseconds) after an electrical field is imposed through the channels. Patankar and Hu (1998) gave out the estimated dimensional time to reach the steady state, $\tau = 0.467 w^2 / \nu$, where w is the width of the channel and ν is the kinematic viscosity of the buffer solution. In the present study, the transient time is about 4.7 ms ($w = 100$ μm, $\nu = 10^{-6}$ m^2/s). This time is usually much smaller than all other related characteristic times in the immunoassay operations, such as sample delivery and incubation, which are of the order of 100 s in the present study. The steady-state simplification greatly reduces the computational time since the flow only needs to be calculated once for a given applied electric field. Another simplification is to decrease the dimensionality of the problem from 3-D to 2-D if all the microchannels of the

chip have a constant depth and the physical properties of the chip substrate and cover plate are assumed to be identical and homogeneous (Ermakov et al. 1998; Cummings et al. 2000). Given these conditions, the electric field and the flow field are truly two-dimensional and independent of the channel depth. Therefore, we will use a 2-D model in the following numerical simulation since the microchannels used here have a constant depth and uniform solid walls.

2.1 Governing equations

Electroosmotic flow generated by an applied electric field is described by the steady incompressible Navier-Stokes equations,

$$\vec{V}_{eo} \cdot \nabla \vec{V}_{eo} = -\frac{1}{\rho_f}\nabla P + v\nabla^2 \vec{V}_{eo} + \frac{\rho_e}{\rho_f}\vec{E} \qquad (1)$$

$$\nabla \cdot \vec{V}_{eo} = 0. \qquad (2)$$

In these equations, $\vec{V}_{eo}$ is the bulk electroosmotic flow field, P is the pressure, v is the kinematic viscosity of the fluid and ρ_f is the density of the fluid.

The driving force of the liquid flow in Eq. (1) is the electrical body force $\rho_e \vec{E}$, where ρ_e is the electrical charge density in the EDL and $\vec{E}$ is the local electric field strength. It should be noted that there is no net charge density in the bulk liquid outside the EDL. Because the buffer solutions have high ionic concentrations (of the order of 10^{-2} M), the EDL thickness is very small (less than 10 nm) in comparison with the size of the microchannels (100 μm). Therefore the details of the flow field within the EDL can be safely neglected; instead, the flow in the EDL can be considered as a slip flow boundary condition for the bulk flow in the microchannel. In the following calculations, the force term $\rho_e \vec{E}$ from Eq. (1) is neglected and the EOF effect is taken into account by introducing the slip boundary conditions at the solid walls. According to the theory of electrostatics, the applied electrical potential, Φ, is described by the Laplace's equation,

$$\nabla^2 \Phi = 0. \qquad (3)$$

The local electric strength can then be calculated by $\vec{E} = -\nabla\Phi$. The slip velocity at the solid walls is the electroosmotic flow velocity,

$$\vec{V}_{slip} = \mu_{eo}\vec{E}, \qquad (4)$$

where $\mu_{eo} = -\varepsilon\varepsilon_0\varsigma/\eta$, is called the electroosmotic mobility, which is the electroosmotic velocity per unit of the applied electric field. Here ϵ is the dielectric constant of the liquid, ϵ_0 is the permittivity in vacuum, ζ is the zeta potential on the channel wall and η is the dynamic viscosity of the liquid.

Once the flow field is determined, the sample concentration is introduced by

$$\frac{\partial C_i}{\partial t} + (\vec{V}_{eo} + \vec{V}_{ep}) \cdot \nabla C_i = D_i\nabla^2 C_i, \qquad (5)$$

where C_i is the concentration of the i-th sample (primary antibody, secondary antibody or washing buffer in the present study), $\vec{V}_{ep}$ is the electrophoretic velocity of the sample given by $\vec{V}_{ep} = \mu_{ep}\vec{E}$, where μ_{ep} is the electrophoretic mobility and D_i is the diffusion coefficient of the i-th sample.

2.2 Numerical algorithm

The most difficult part of the simulation is to solve the Navier-Stokes equations (1) and (2) because of the nonlinear convection term. Unlike the compressible counterpart, the incompressible Naiver-Stokes equations do not have an explicit expression for the pressure. The pressure can only be obtained by imposing the divergence-free condition (Eq. (2)) for the velocity field. We adopt the augmented Lagrangian method (Bertsekas 1982) to solve Eqs. (1) and (2) using the iterative procedure,

$$\vec{V}_{eo}^n \cdot \nabla \vec{V}_{eo}^{n+1} = -\frac{1}{\rho_f}\nabla P^{n+1} + v\nabla^2 \vec{V}_{eo}^{n+1}$$
$$P^{n+1} = P^n - \beta\nabla \cdot \vec{V}_{eo}^{n+1}, \qquad (6)$$

where β is the augmented Lagrangian parameter, and set to 20 in all computations. The superscripts $n+1$ and n represent the values at current computational steps and previous steps, separately. The algorithm, if converging, does not introduce any further error and provides an answer for the pressure.

The sample concentration Eq. (5) is a transient advection-diffusion type equation. We use the implicit Euler backward scheme,

$$\frac{C_i^{n+1} - C_i^n}{\Delta t} + (\vec{V}_{eo} + \vec{V}_{ep}) \cdot \nabla C_i^{n+1} = D_i\nabla^2 C_i^{n+1} \qquad (7)$$

where Δt is the time step. A desirable large Δt can be used in our simulations because of the implicit scheme.

We employ the finite element method (FEM) to approximate the Eqs. (3), (6) and (7). Computational domain is divided into a set of unstructured six-node triangular finite elements, which allow great flexibility to solve the flow field and sample transportation within any complex layout of the microchannel system. Currently we chose quadratic piecewise polynomials for $\vec{V}_{eo}$, Φ and C_i and linear piecewise polynomials for P. This is the same mixed element discretization used by Taylor and Hood (1973) in FEM simulation for Navier-Stokes equations. The discretized systems of algebraic equations are solved using an incomplete LU factorization preconditioned Bi-CGSTAB solver (van der Vorst 1992).

2.3 Boundary conditions

Boundary conditions for the Eqs. (3), (6) and (7) are given as follows,

$$\text{at inflow ends}\quad \Phi = \Phi_i,\quad \frac{\partial \vec{V}_{eo}}{\partial n} = 0,\quad P = 0,\quad C_i = C_{i0}$$

$$\text{at outflow ends}\quad \Phi = \Phi_i,\quad \frac{\partial \vec{V}_{eo}}{\partial n} = 0,\quad P = 0,\quad \frac{\partial C_i}{\partial n} = 0$$

$$\text{at walls}\quad \frac{\partial \Phi}{\partial n} = 0,\quad \vec{V}_{eo} = \vec{V}_{slip},\quad \frac{\partial P}{\partial n} = 0,\quad \frac{\partial C_i}{\partial n} = 0,$$

where Φ_i are the different electrical voltages applied on the electrodes in the reservoirs. Whether an end is an inflow or outflow boundary is decided by the direction of flow velocity. If the flow is entering the channel, the boundary is an inflow boundary. Otherwise, it is an outflow boundary. In the computation of the sample concentration, the distribution of concentration obtained from the previous operation will be used as the initial condition of the next operation.

3 Experimental section

3.1 Reagents and solutions

Helicobactes pylori (antigen) was cultured and lysed in the Sherman Lab, at the Hospital for Sick Children, Toronto, Canada, following the procedure described in the paper of Lin et al. (2004). The lysed antigen was then diluted to concentrations of 1, 10, 100 ng/μL by using a coating buffer that consists of 0.03 M of $NaHCO_3$ and 0.02 M of Na_2CO_3 at pH 9.6. Blocking buffer is 25 mM tris–HCl solution containing 5% bovine serum albumin (BSA) titrated to pH 7.5. For *H. pylori* antigen detection, commercially available polyclonal rabbit anti-*H. pylori* antibody (DAKO, Denmark) and rhodamine(TRITC)-conjugated donkey anti-rabbit IgG (Jackson ImmunoResearch Laboratories Inc, USA) were used as the primary antibody and the secondary antibody, respectively, in the form of dilution of 1:25 in blocking buffer. Twenty-five mM tris–HCl solution also acts as washing buffer solution.

3.2 Fabrication of PDMS chip

The master was fabricated using a rapid prototyping/soft-lithography technique (Duffy et al. 1998). Details can be found in the paper of Biddiss et al. (2004). A 15:1 well-mixed mixture of PDMS prepolymer and curing agent (Dow Corning, USA) was poured over the master and cured at 75°C for about 4 h after being degassed under low vacuum. After curing, the PDMS replica was peeled from the master and sealed against a glass slide after oxygen plasma treating for 30 s. Solution reservoirs (wells) were formed by boring 4.5 mm i.d. holes at each end of the microchannels in the PDMS slab.

3.3 Immobilization of antigen

We adopted the passive adsorption procedure to immobilize the antigen onto the PDMS microchannel wall, taking the advantage of the high surface-to-volume ratio of microchannels. Ten μL diluted *H. Pylori* antigen was added to one reservoir and filled into all the channels rapidly due to the capillary effect. The antigen was immobilized onto the channel surface and incubated for 2 h under room temperature. All the channels were then washed by tris–HCl and filled with blocking buffer for another 15 min to prevent the non-specific protein reaction. The chip was then ready for the immunoassay analysis through fully automated microfluidic operations.

3.4 Electrokinetic control

The sequential operations of microfluidic transportation are realized by using the LabSmith HVS448 High Voltage Sequencer (Labsmith, USA). This power supply, controlled by monitoring software in Windows, can provide eight high-voltage channels simultaneously with a programmable sequence. It has the ability to switch voltages rapidly through different modes and settings.

3.5 Detection principle

In our studies, the primary rabbit anti- *H. pylori* antibody was captured by the immobilized antigen on the channel surface, and then detected with the secondary rhodamine-conjugated anti-rabbit IgG. Finally, the
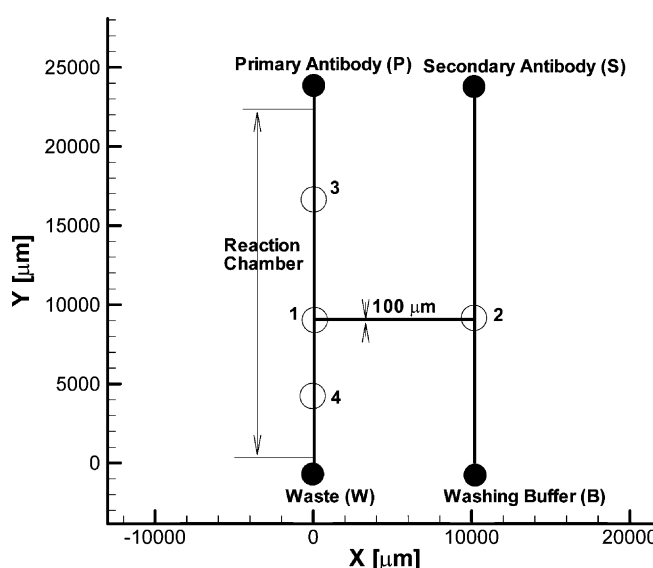

Fig. 1 Layout of a microfluidic ELISA chip. All the channels are 100 μm wide and 20 μm deep. Overall outer dimensions of the chip are 23 ×10 mm. The diameter of all the reservoirs is 4.5 mm (not proportional to the exact size)

Table 1 Operation steps and parameters for a full immunoassay analysis cycle

Step	Applied potentials at reservoirs (V)				Duration of the step (s)
	Φ_W	Φ_B	Φ_S	Φ_P	
Dispensing (P)	0	95	100	250	210
Incubating (P)	0	47.5	50	125	300
Washing (P)	0	500	300	0	120
Dispensing (S)	0	265	500	0	350
Incubating (S)	0	132.5	250	0	300
Washing (S)	0	500	0	0	300

Table 2 Normal inflow/outflow velocity and volume change in each reservoir at each operation step

Step	Velocity (μm/s) /Volume change (nL)			
	W	B	S	P
Dispensing (P)	+140/+58.8	+3/+1.3	−2/−0.9	−141/−59.2
Incubating (P)	+70/+42.0	+1.5/+0.9	−1/−0.6	−70.5/−42.3
Washing (P)	+159/38.2	−271/−65.0	+10/+2.4	+102/+24.4
Dispensing (S)	+133/93.1	+2/+1.4	−221/−154.7	+86/+60.2
Incubating (S)	+66.5/39.9	+1/+0.6	−110.5/−66.3	+43/+25.8
Washing (S)	+114/68.4	−396/−237.6	+208/+124.8	+74/+44.4
Total (nL)	+340.4	−298.4	−95.3	+53.3

Sign +/− represents inflow/outflow velocity and gain/loss of fluid.

rhodamine-labeled secondary antibody would bind to the primary antibody on the solid wall of the reaction chamber. The chip was observed under a Leica DM-LB fluorescence microscope (Leica Microsystems Canada) and the images were captured by using a Retiga 12-bit cooled CCD camera. Images were quantified by Open-Lab 3.1.5 imaging software of the Leica fluorescence microscope at an exposure time of 2 s.
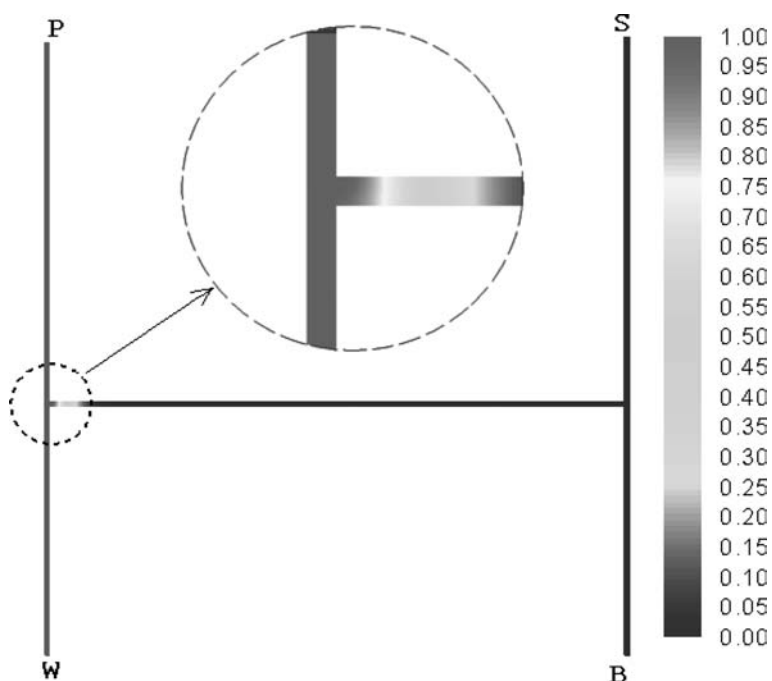

Fig. 2 The path of the sample transportation in the sequential operation steps of the immunoassay. **a** Dispensing of the primary antibody and incubating. **b** Washing of the primary antibody. **c** Dispensing of the secondary antibody and incubating. **d** Washing of the secondary antibody
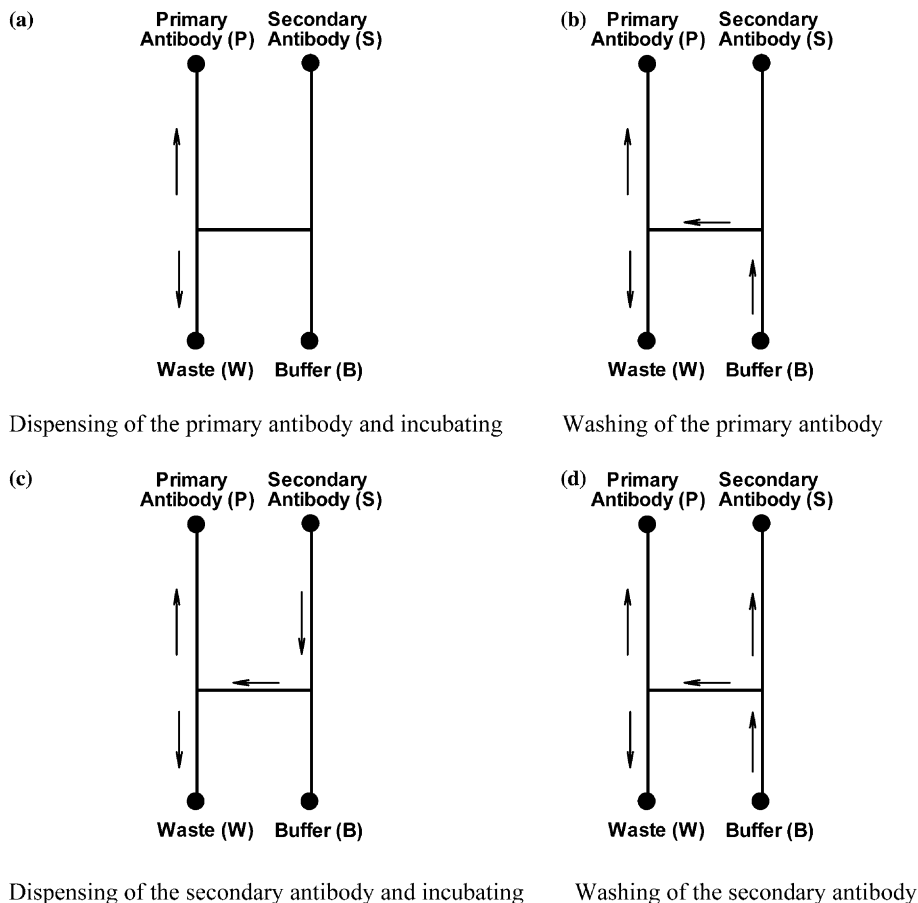
4 Results and discussion

An H-shaped microfluidic network for the immunoassay chip in the present work is shown in Fig. 1. All the microchannels have a width of 100 μm and a uniform depth of 20 μm. The outer dimensions of the chip are 23 ×10 mm. Four 4.5 mm i.d. circular wells are connected to the four ends of the microchannels as the solution reservoirs. In the experiments, initially, the buffer reservoir, the waste reservoir and the channels were filled with the washing buffer solution while the other two reservoirs were filled with 12 μL primary antibody and secondary antibody solutions, respectively. Platinum electrodes were inserted into these reservoirs to set up the electrical field across the channels. Different electric potentials at different times were applied to control the operation procedures of the

Fig. 3 The delivery of the primary antibody and the secondary antibody. The colors present the normalized sample concentrations. **a** Dispensing of the primary antibody, $\tau = 210$ s. **b** Dispensing of the secondary antibody, $\tau = 380$ s

(a) Dispensing of the primary antibody, τ=210 s
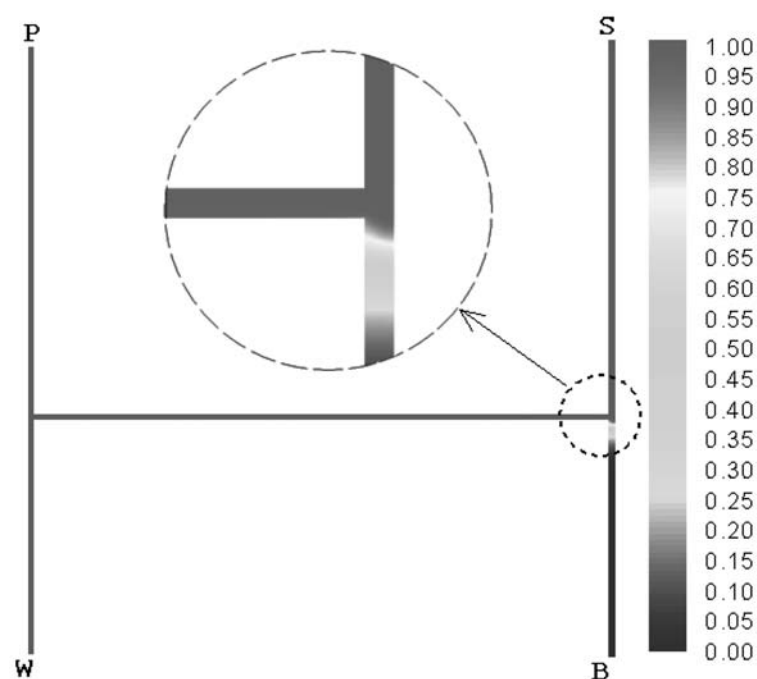
(b) Dispensing of the secondary antibody, τ=380 s

immunoassay analysis. The exact configuration in Fig. 1 is used in both numerical simulations and experiments. In Fig. 1, the small circles with a number denote the positions for fluorescent images taken under microscope as discussed later.

We considered the following requirements in the design of the microfluidic immunoassay chip:

1. The channels should be as short as possible to minimize transport distance and reagent consumptions, but long enough to avoid cross-contamination among the samples due to long-time diffusion effect.
2. The microfluidic network should include at least one supply channel and one reservoir for each sample and washing buffer, to avoid cross-contamination. The number of reservoirs (each with one electrode) should be as small as possible because the more the number of applied potentials, the more difficult to control a designated operation, such as controlling the flow direction in one or two channels while the liquid in other channels remains stationary. The designed chip in Fig. 1 has the minimal number of the reservoirs for the required microfluidic functions.

3. The size of reservoirs, especially the reservoirs of buffer solution and waste, should be large enough to minimize the effects of hydrostatic pressure-driven flow. The unequal liquid levels in different reservoirs will cause pressure-driven flows that will interfere with the desired electrokinetically-driven flows. We address this problem in detail later.
4. The cross-section of microchannels should be large enough to carry a detectable volume of reagents but as small as possible to reduce the Joule heating effect (Erickson et al. 2003). High temperature caused by Joule heating may not only affect the flow but also impair the immunoassay. In this study, we choose a cross-section of 100×20 μm for all the channels. We also limit the electrical field strength to 200 V/cm to reduce the heat generation.

The most challenging aspect in our present immunoassay chip is how to achieve the automatic, electrokinetic flow control, not only with spatial precision but also with temporal precision. These flow controls include flow switching and reagent holding in the reservoirs. For example, when the primary antibody is driven

Fig. 4 The fluorescent images from the detection of 100 ng/μL *H. Pylori* antigen. The images are taken using a 32X lens at an exposure time of 2 s. **a** Positive reaction at position 1. **b** Negative control at position 2. **c** Positive reaction at position 3. **d** Positive reaction at position 4
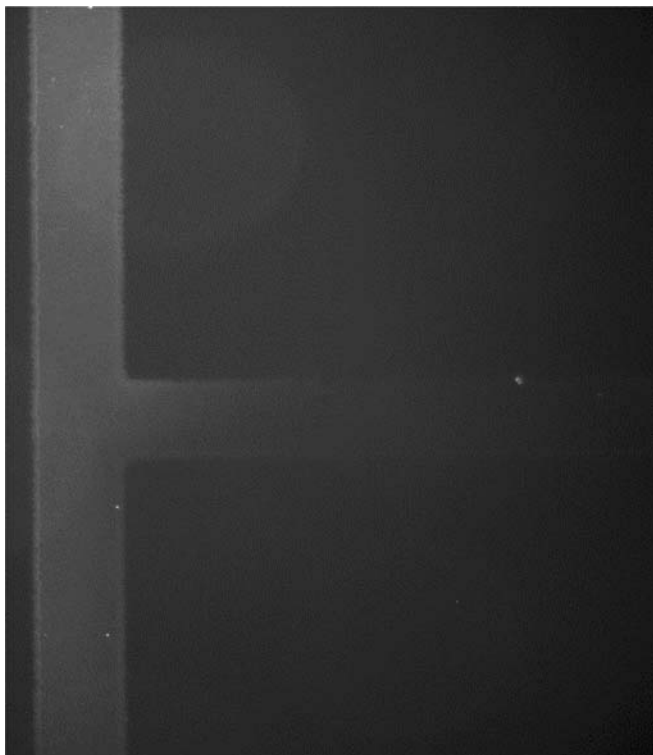
Positive reaction at position 1

Negative control at position 2

Positive reaction at position 3

Positive reaction at position 4
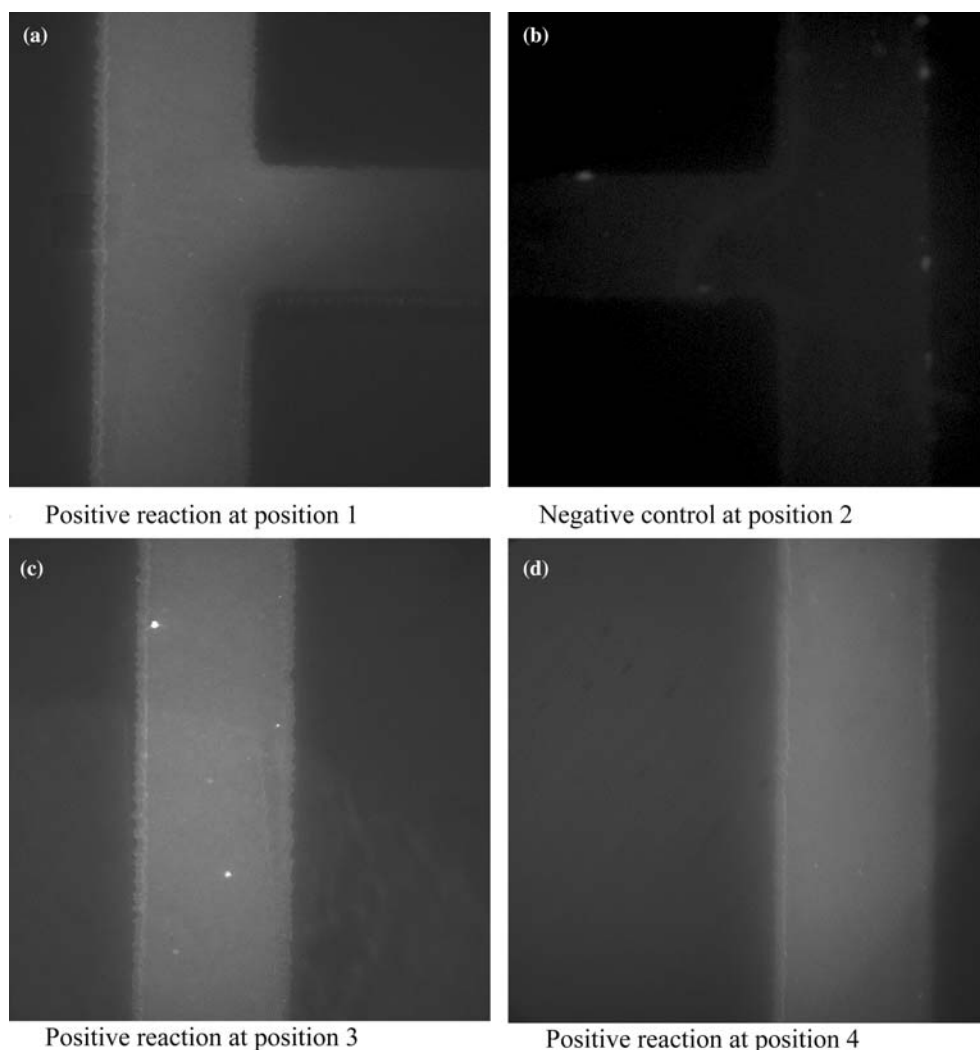
Fig. 5 A larger viewing area around position 1 taken by a 10× lens

into the reaction chamber, the secondary antibody and the washing buffer should be held stationary in their reservoirs. Similarly, when the secondary antibody is loaded into the reaction chamber the primary antibody and washing buffer should be still held in their reservoirs. Additionally, these sequential loading and washing operations require accurate flow switching. Such
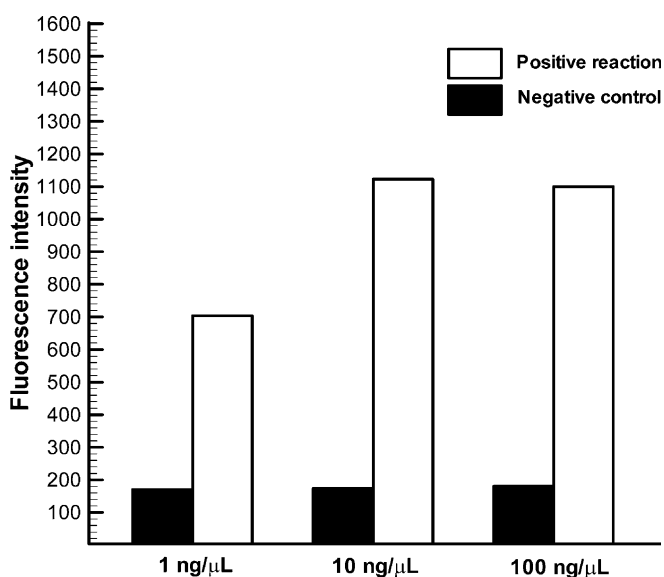

Fig. 6 Comparison of the fluorescence intensity of positive reaction and negative control for different concentration antigen

precise and automatic manipulation of pre-loaded multiple reagents in a microchannel network requires accurate control of the applied electric fields and the duration of each step before the experiments. Therefore, we have to find the applied voltages and duration of each operation for the given microchip by numerical simulation first and then apply them to control the experiments.

4.1 Numerical results

In our simulations, we choose an electroosmotic mobility of 1.3×10^{-4} cm^2/(Vs), which is measured experimentally by the well-established current monitoring technique (Huang et al. 1988; Sze et al. 2003), in the antigen-coated microchannel, a kinematic viscosity of 1.0×10^{-2} cm^2/s and a diffusion coefficient of 3×10^{-6} cm^2/s for all the samples. By measuring the fluorescence-conjugated antibody, we also found that all the samples are almost electrically neutral, i.e., $\mu_{ep}=0$, therefore, we can ignore the electrophoretic effect on the sample transport.

For simplicity, we denote the primary antibody, the secondary antibody, the washing buffer solution and the waste by P, S, B and W, respectively in the following discussion. Table 1 describes the operation steps for a full analysis cycle in the present immunoassay chip. All the voltages listed here are carefully tuned by the numerical experiments. The total time for a complete immunoassay test is 26 min and 20 s.

Figure 2 indicates the path of the sample transportation in each operation step. It is worth noting that flows during incubating steps have the same path as that in dispensing steps so that the incubation is realized in a continuous-flow way rather than the stagnant way usually used in the conventional immunoassay. We have found that the tolerable fluctuation of the applied voltages could be up to ±5%. Figure 3 displays the transportation of the primary antibody at τ=210 s and secondary antibody at τ=980 s. Due to the large ratio of the microchannel length to width, we only draw a part of the chip that is enough to illustrate the flow pattern. As shown in Fig. 3a, we applied the electric potential to allow slight leakage of the primary antibody from the reaction chamber (the whole left arm) into the horizontal channel so that the antibody concentration was uniform within the reaction chamber. A similar tactic was used to keep the evenness of the secondary antibody in the reaction chamber, as shown in Fig. 3b. Predictably, the positive reaction will happen only in the channel regions that have both antibodies, as shown in Fig. 3a, b. Other sections of the microchannel network can be considered as the negative control because there is no primary antibody and hence no reaction. The following experiments will demonstrate such phenomenon.

During the microfluidic immunoassay operation, some reservoirs receive liquid while other reservoirs lose liquid. The height difference between the liquid levels in these reservoirs will cause pressure-driven flow, which can significantly disturb the precise delivery of the

	Microfluidic immunoassay	Conventional ELISA
Incubation time	5 min	1 h
Total assay time	26 min	~3 h
Reagent consumption	100–220 nL (in channel) 12 μL (in reservoirs)	~100 μL
Limit of detection	1 ng/μL	10 ng/μL
Reagent delivery	Flow-through (automated electrokinetically-driven)	Pipetting

reagents if it is sufficiently large compared to the electroosmotic flow. Sinton and Li (2003) have demonstrated that a height difference of only 600 μm over a 15 cm distance would generate a velocity of 100 μm/s in a 200 μm i.d. circular channel.

Because at each step the flow field is steady, we can use following formula to estimate the change of the fluid volume in each reservoir,

$$VC = Q\tau = U_n wh\tau$$

where Q is the flow rate, U_n is the normal velocity measured at the inflow/outflow boundary, w and h are the width and depth of the channel, respectively and τ is the operation duration. The velocities and volume changes at each reservoir are presented in Table 2. Table 2 shows that the total inflow volume is identical to the total outflow volume at each step, which confirms that the present numerical scheme meets the mass conservation requirement.

The largest height difference Δh occurs between reservoirs W and B and is approximately 40 μm. The hydraulic resistance of a rectangular microchannel with a large aspect ratio (i.e., $w >> h$) can be found by (Crowther 2001)

$$R = \frac{12\eta L}{wh^3} \qquad (8)$$

where L is the distance between two reservoirs. Using the relation of $Q = \Delta P/R$, the average speed of the pressure-driven flow $\bar{V}_{pd}$ induced by a pressure drop is linked to Δh by

$$\bar{V}_{pd} = \frac{\Delta h}{L} \cdot \frac{\rho_f g h^2}{12\eta} \qquad (9)$$

For the present case, $\bar{V}_{pd}$ is only about 0.5 μm/s for the height difference of 40 μm over a distance of 28 mm between the reservoirs W and B and therefore the effect of pressure-driven flow can be safely neglected.

From Table 2, we can also estimate the actual consumptions of the primary antibody and the secondary antibody as about 100 and 220 nL, which are much less than that required in the conventional immunoassay test (usually 100 μL).

4.2 Experimental results

After the immobilization of the *H. Pylori* antigen and the blocking step described previously, the immunoassay experiments were carried out at room temperature. The sequential microfluidic operations were controlled by the High Voltage Sequencer based on the voltages and times designed by numerical simulations. The total assay process lasts approximately 26 min, without any manual operation.

Figure 4 shows the fluorescent images for the detection of 100 ng/μL *H. Pylori* antigen taken by a 32× lens on the positions numbered in Fig. 1. The positive reaction is very uniform within the reaction chamber, which demonstrates that the samples are delivered evenly by the electrokinetic flow. Compared to the negative control image at position 2, the signal of the positive reaction is strong enough to be identified. Figure 5 gives a picture of a larger viewing area taken by using a 10× lens around the left T-shaped intersection. As seen from Fig. 5, there exists a sharp decrease of the fluorescent signal from the vertical channel into the horizontal channel, which corresponds to a transition from a positive reaction to a negative control. This is in good agreement with the predicted primary antibody concentration field by the numerical simulation, as shown in Fig. 3a.

Nonspecific protein adsorption is a common problem that limits the detection sensitivity in the heterogeneous immunoassays. We used 25 mM tris–HCl solution containing 5% BSA as the blocking buffer and found that it could effectively alleviate the nonspecific binding problem and thus improve the detection quality. Figure 6 compares the signal magnitudes of the positive reaction and the negative control for different concentrations of the coating antigen. The fluorescence intensity was obtained by quantifying the 12-bit digital images by OpenLab 3.1.5 software of the Leica fluorescence microscope. The big signal ratio of the positive reaction to the negative control demonstrates that this microfluidic immunoassay chip is capable of detecting as low as 1 ng/μL *H. pylori* antigen, which is comparable to or even better than the detection limit in a conventional ELISA or pressure-driven ELISA (Lin et al. 2004). Table 3 compares our present immunoassay chip with the conventional ELISA and clearly shows that our chip achieves shortened assay time, less reagent consumption and even lower limit of detection. Using other more sensitive detection methods such as chemiluminescence and absorbance (Sia et al. 2004), we can achieve even lower limits of detection on the present immunoassay chip.

5 Conclusions

We have developed a theoretical model and conducted the numerical simulations for the sequential operations

involved in a microfluidic immunoassay chip. Based on the parameters obtained by the numerical experiments, we designed a fully automated prototype of microfluidic chip for heterogeneous immunoassay. The reagent solutions are successfully guided to the reaction chamber through electrokinetically driven flow and thus the sequential assay operations can be achieved by adjusting the applied voltages in a temporal order. In our chip design, we also carefully considered and minimized the effect of the induced pressure-driven flow caused by the height differences of the fluid level in the reservoirs. We have carried out the immunoassay experiments to detect *H. pylori* antigen and found that our microfluidic chips have comparable, if not better, limits of detection, to the conventional ELISA.

References

Arulanandam S, Li D (2000) Liquid transport in rectangular microchannels by electroosmotic pumping. Colloid Surface A 161:89–102

Bertsekas DP (1982) Constrained optimization and Lagrange multiplier methods. Academic, New York

Biddiss E, Erickson D, Li D (2004) Heterogeneous surface charge enhanced micro-mixing for electrokinetic flows. Anal Chem 76:3208–3213

Chiem N, Harrison DJ (1998) Microchip systems for immunoassay: an integrated immunoreactor with electrophoretic separation for serum theophylline determination. Clin Chem 44:591–598

Crowther JR (2001) The ELISA guidebook. Humana Press, New Jersey

Cummings EB, Griffiths SK, Nilson RH, Paul PH (2000) Conditions for similitude between the fluid velocity and electric field in electroosmotic flow. Anal Chem 72:2526–2532

Dodge A, Fluri K, Verpoorte E, de Rooij NF (2001) Electrokinetically driven microfluidic chips with surface-modified chambers for heterogeneous immunoassays. Anal Chem 73:3400–3409

Duffy DC, McDonald JC, Schueller OJA, Whitesides GM (1998) Rapid prototyping of microfluidic systems in poly(dimethylsiloxane). Anal Chem 70:4974–4984

Ekins RP (1960) The estimation of thyroxine in human plasma by an electrophoretic technique. Clin Chim Acta 5:453–459

Erickson D, Li D (2003) Three-dimensional structure of electroosmotic flow over heterogeneous surfaces. J Phys Chem B 107:12212–12220

Erickson D, Sinton D, Li D (2003) Joule heating and heat transfer in poly(dimethylsiloxane) microfluidic systems. Lab Chip 3:141–149

Ermakov SV, Jacobson SC, Ramsey JM (1998) Computer simulations of electrokinetic transport in microfabricated channel structures. Anal Chem 70:4494–4504

Harrison DJ, Fluri K, Seiler K, Fan Z, Effenhauser CS, Manz A (1993) Micromachining a miniaturized capillary electrophoresis-based chemical analysis system on a chip. Science 261:895–897

Huang X, Gordon MJ, Zare R(1988) Current-monitoring method for measuring the electroosmotic flow rate in capillary zone electrophoresis. Anal Chem 60:1837–1838

Knight Honey J (2002) I shrunk the lab. Nature 418:474–475

Kovacs G (2001) Micromachined transducers sourcebook. McGraw-Hill, Boston

Lai S, Wang S, Luo J, Lee LJ, Yang ST, Madou MJ (2004) Design of a compact disk-like microfluidic platform for enzyme-linked immunosorbent assay. Anal Chem 76:1832–1837

Lin FYH, Sabri M, Erickson D, Alirezaie J, Li D, Sherman PM (2004) Development of a microchannel immunoassay for the detection of Helicobacter pylori infection and colourimetric quantitation of microchannel immunoreaction. Analyst 129:823–828

Linder V, Verpoorte E, de Rooij NF, Sigrist H, Thormann W (2002) Application of surface biopassivated disposable poly(dimethylsiloxane)/glass chips to a heterogeneous competitive human serum immunoglobulin G immunoassay with incorporated internal standard. Electrophoresis 23:740–749

Patankar NA, Hu HH (1998) Numerical simulation of electroosmotic flow. Anal Chem 70:1870–1881

Sia SK, Whitesides GM (2003) Microfluidic devices fabricated in poly(dimethylsiloxane) for biological studies. Electrophoresis 24:3563–3576

Sia SK, Linder V, Parviz BA, Siegel A, Whitesides GM (2004) An integrated approach to a portable and low-cost immunoassay for resource-poor settings. Angew Chem Int Ed 43:498–502

Sinton D, Li D (2003) Electroosmotic velocity profiles in microchannels. Colloid Surface A 222:273–283

Stewart K, Griffith SK, Nilson RH (2001) Low-dispersion turns and junctions for microchannel systems. Anal Chem 73:272–278

Sze A, Erickson D, Ren L, Li D (2003) Zeta-potential measurement using Smoluchowski equation and the slope of current-time relationship in electroosmotic flow. J Colloid Interface Sci 261:402–410

Taylor C, Hood P (1973) A numerical solution of the Navier-Stokes equations using the finite element method. J Comp Phys 1:73–100

van der Vorst HA (1992) Bi-CGSTAB: A fast and smoothly converging variant of Bi-CG for the solution of nonsymmetric linear systems. SIAM J Sci Stat Comput 13:631–644

Wang J, Ibanez A, Chatrathi MP, Escarpa A (2001) Electrochemical enzyme immunoassays on Microchip Platforms. Anal Chem 73:5323–5327

Yalow RS, Berson SA (1959) Assay of plasma insulin in human subjects by immunological methods. Nature 184:648–1649